ACS OMEGA

Article

http://pubs.acs.org/journal/acsodf

Systematic Analysis of Poly(*o*-aminophenol) Humidity Sensors

Salma Bibi,[†] Salma Bilal,*[,†] Anwar-ul-Haq Ali Shah,*[,‡] and Habib Ullah[§]

[†]National Centre of Excellence in Physical Chemistry, University of Peshawar, 25120 Peshawar, Pakistan

[‡]Institute of Chemical Sciences, University of Peshawar, 25120 Peshawar, Pakistan

[§]Environment and Sustainability Institute (ESI), University of Exeter, Penryn Campus, Penryn, Cornwall TR10 9FE, United Kingdom

Supporting Information

ABSTRACT: A thin film of poly(*o*-aminophenol), POAP, has been used as a sensor for various types of toxic and nontoxic gases: a gateway between the digital and physical worlds. We have carried out a systematic mechanistic investigation of POAP as a humidity sensor; how does it sense different gases? POAP has several convenient features such as flexibility, transparency, and suitability for large-scale manufacturing. With an appropriate theoretical method, molecular oligomers of POAP, NH and O functional groups and the perpendicular side of the polymeric body, are considered as attacking sites for humidity sensing. It is found that the NH position of the polymer acts as an electrophilic center: able to accept electronic cloud density and energetically more favorable compared to the O site. The O site acts as a nucleophilic center and donates electronic cloud density toward H_2Ovap. In conclusion, only these two sites are involved in the sensing process which leads to strong intermolecular hydrogen bonding, having a 1.96 Å bond distance and $\Delta E \sim -35$ kcal mol^{-1}. The results suggest that the sensitivity of the sensor improved with the oxidization state of POAP.

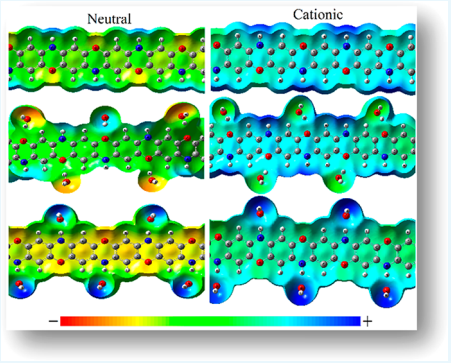

1. INTRODUCTION

Conducting polymers (CPs) are becoming an active field of research which has brought a dynamic revolution in the field of chemistry, physics, and engineering in the last several decades.[1] Electrical conductance along the tailorable structure of CPs, followed by optical and electronic properties, has proven their potential application in a large number of organic electronics such as batteries,[2] fuel cells,[3,4] solar cells,[5] light emitting diodes,[6] supercapacitors,[7] and optical displays.[8,9] The most widely used CPs are polyaniline (PANI),[10] polypyrrole (PPy),[11] polythiophene (PT),[12] poly(*o*-phenylenediamine) (POPD),[13] and poly(*o*-aminophenol) (POAP).[14]

Besides these technological applications, CPs are getting a valuable position in the design of gas sensing devices. Humidity control is a grand challenge in various sensitive industries such as packed food, storage of drugs, preventing different antiques and paintings, agricultural uses, and in environmental control.[15−17] Although humidity sensors are available in the market, based on dew point,[18] catalysis,[19,20] infrared,[21] and inorganic semiconductor (Ti, Zn) sensors,[19,22] most of them require high operation temperature, show deviation from the linear response, and create problems in reversibility. Cost maintenance and high power consumption restrict their viability and versatility.[23] Lots of research is in progress to overcome these drawbacks and develop an effective material for humidity sensing.

One of the best options is to replace other inorganic materials with flexible CPs. CPs are stable and cheap, require low operational temperature, have low weight, and are easily synthesizable with good reversibility and tailorable properties; this make them prominent compared to other inorganic materials.[1,24−27] Some of the most commonly used CPs in the field of humidity sensing are PANI,[28−30] POPD,[31,32] and PPy,[33−35] which have been used in different oxidation states. Furthermore, they are either employed in pure, blended, or in composites form with other inorganic materials to enhance their sensitivity, flexibility, and selectivity.[36] Scientists are investigating varieties of CPs to be the best humidity sensing materials, but they are facing numerous issues such as formation of a nonuniform, unstable, and adhesive film on the electrode.[17] POAP is a redox conducting polymer with the unique ability to have a uniform, stable, and adhesive film formation besides its other electroactive properties.[37] POAP is a substituted derivative of PANI, where the structure has two potentially active sites (NH and O positions) for the interaction of H_2Ovap and other related gases. It is recently reported that a modified POAP film has improved sensing properties, compared to other CPs.[38−40] Although POAP has been experimentally reported as a sensor, no one has paid attention to its mechanistic study; which functional group is more sensitive and how does it attract gas particles?

In this work, we employed density functional theory (DFT) and time-dependent (TD) DFT simulations at various level of theories to find out the best method for precise correlation of theory with the already experimental evidence of POAP. Molecular oligomers of POAP, both reduced and oxidized,

Received: July 19, 2017
Accepted: September 20, 2017
Published: October 5, 2017

DOI: 10.1021/acsomega.7b01027
ACS Omega 2017, 2, 6380−6390

with different chain lengths are considered where the NH and O functional groups and perpendicular sides of the polymeric body are considered as attacking sites toward humidity sensing. The sensing phenomenon is investigated from structural distortion (change in geometric parameters), intermolecular interaction energies, natural bonding orbital analysis (NBO), and electronic property simulations such as HOMO, LUMO, density of states, band gap, electrostatic potential, and UV−vis spectral analysis. Moreover, the current theoretical investigation of POAP, combined with the already reported behavior of POAP, will lead to the fabrication of a proficient and competent humidity and other related gas sensor.

2. RESULTS AND DISCUSSIONS

a. Selection of Level of Theory. DFT analysis at various levels of theory is carried on the symmetrical 3PAOP (Figure 1)

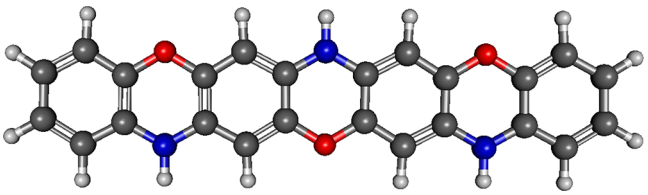

Figure 1. Optimized geometric structure of symmetric 3POAP.

to find the best, inexpensive method for precisely correlating the theory with experiment. Results of ten different levels of theory on the symmetrical 3POAP are listed in Table 1, which led us to conclude that B3LYP/6-31G(d) is the best regarding both the computational time and accuracy points of view.

DFT at the B3LYP/6-31G(d) level of theory not only reproduces the experimental band gap[41,42] but is very fast and cheap regarding the computational point of view. The difference of 0.28 eV between the experimental and simulated band gap is due to the fact that the observed one was from the thin film while the calculation is that of the gas phase.

b. Selection of Proper Interacting System(s). *i. Optimized Geometric Parameters.* Geometry optimization of all these species has been performed using DFT at the 6-31G (d) level of theory. The sensing potential of *n*POAP toward water vapors (H_2O_{vap}) is estimated from the geometrical distortion of the polymeric backbone, interacting with water vapor(s). These parameters include intermolecular distance, intermolecular bond length, bond angles, and dihedral angles of POAP. Optimized geometries of 4POAP and their complexes with H_2O at different sides have been shown in Figures 2 and S1−3, while their different geometric parameters are listed in Table 2. We have selected different models to find the best interaction between H_2O and 4POAP, where the H_2O either interacts at NH (Figure 1), O (Figure S1), perpendicular to the backbone (Figure S2), or considering both the NH and O sides of 4POAP (Figure S3). Results and discussion of the latter two interacting systems show that instead of interaction with the polymeric body of 4POAP, water molecules hydrogen bond among themselves, as can be seen from Figures S2 and S3 of the Supporting Information. So, the overall interaction in these species is comparatively low as that of H_2O attached at NH or O functional groups. In case of the 4POAP_NH@H_2O system, one, two, and three NH sites of 4POAP were alternatively covered with H_2O and it was found that the O of H_2O makes an intermolecular bond of about 1.95 Å with the H of NH in all these complexes.

A similar but less pronounced intermolecular hydrogen bonding is observed in 4POAP_O@H_2O systems (Figure S1), where the H-bonding is because of the H of H_2O and O of the O site of 4POAP backbone. In summary, both the NH and O sites of 4POAP has a strong interaction with water vapor as can be seen from the strong H-bonding and its distorted geometric structure (Figures 1 and S1).

ii. Interaction Energy, NBO Charge, and Electronic Properties. As a universal solvent, water act as either a proton donor or a proton acceptor which directly depends on the other reactant. In acids/bases, the proton is that of the H^+ ion so, water acts as a proton donor when it reacts with a base; however, it accepts proton when it reacts with an acid. A similar situation is observed, on considering NH and O sites of POAP for water vapor. In the case of H···O, where the H of H_2O react with O of POAP oligomer which withdraw the electronic cloud density of 0.012 e^- from its backbone. On considering two H_2O molecules for the O site of 4POAP, water vapor withdraws about 0.014 e^- of charge, and 0.025 e^- in the case of three H_2O. When water vapor was reacted at the NH sites of 4POAP, it donates electronic cloud density toward the polymer as can be seen from Table 2. 4POAP has withdrawn a charge about 3-fold greater than the NBO charge compared to the O site of POAP. On considering the perpendicular attachment of water vapors, a less pronounced situation is observed where H_2O withdraws electronic cloud density of 0.008 e^-. In this interaction, water molecules circulate around the polymeric body and search for either O or NH groups and forms intermolecular H-bonding through self-interaction.

Table 1. Different Levels of Theory and Their Simulated Total Energy (a.u), HOMO, LUMO, Band Gap (eV), and Time Consumed (min)[a]

no.	functional	basis set	total energy	HOMO	LUMO	band gap	time
1	B3LYP	6-31G(d)	−953.08	−4.16	−0.34	3.82	15
2	B3LYP	6-31G(d, p)	−953.10	−4.17	−0.35	3.82	16
3	B3PW91	6-31G(d, p)	−952.74	−4.25	−0.45	3.80	18
4	BPV86	6-31G(d, p)	−953.16	−3.60	−1.21	2.39	25
5	CAM-B3LYP	6-31G(d, p)	−952.62	−5.42	+0.92	6.34	34
6	HSEH	6-31G(d, p)	−952.11	−4.00	−0.60	3.40	35
7	LSDA	6-31G(d, p)	−947.86	−4.08	−1.75	2.33	22
8	PBE	6-31G(d, p)	−951.97	−3.49	−1.12	2.37	17
9	TPSS	6-31G(d, p)	−953.27	−3.49	−0.97	2.52	22
10	WB97XD	6-31G(d, p)	−952.79	−6.01	+1.45	7.46	21
11	experimental					3.54[41]	

[a]Using 3POAP as a model at fixed memory of 10 GB and 4 processors.

DOI: 10.1021/acsomega.7b01027
ACS Omega 2017, 2, 6380−6390

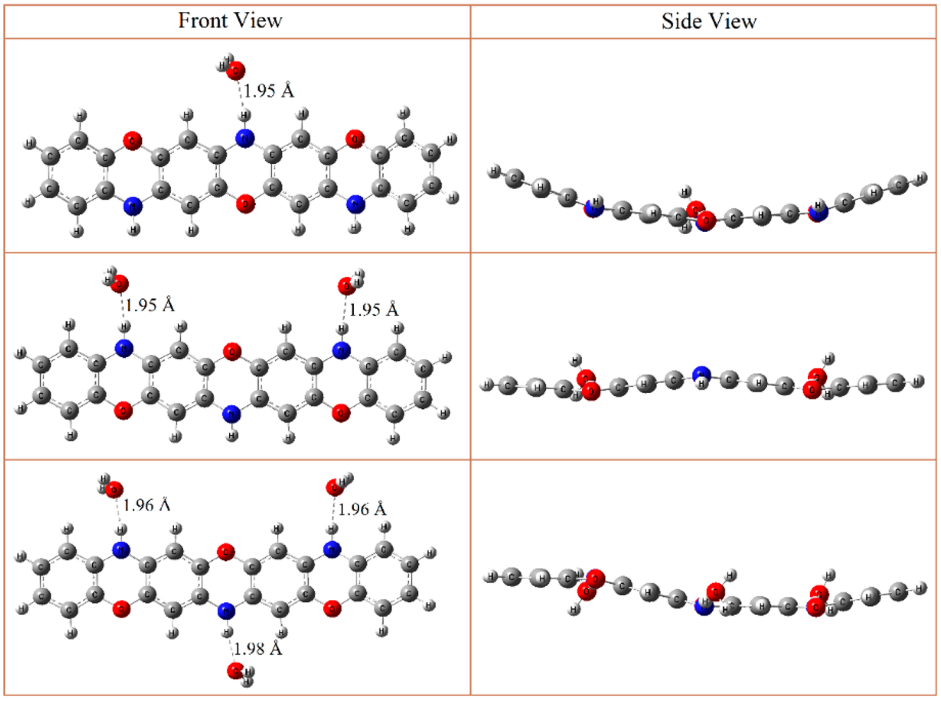

Figure 2. Hydrogen-terminated 4POAP_NH@H_2O.

Table 2. Interaction Energy (kcal mol^{-1}), NBO Charge (e^-), Band Gap (eV), and First Allowed Excitation Energy of 4POAP and Its Complex with H_2O

no.	species	ΔE_{int}	Q_{NBO}	band gap	E_{excit} (eV)
1	4POAP		0	3.54	3.42 (0.57)
2	4POAP_O@1H_2O	−8.22	0.012	3.86	3.63 (0.41)
3	4POAP_O@2H_2O	−14.93	0.014	3.81	3.62 (0.48)
4	4POAP_O@3H_2O	−21.96	0.025	3.88	3.67 (0.41)
5	4POAP_NH@1H_2O	−9.03	−0.032	3.69	3.51 (0.47)
6	4POAP_NH@2H_2O	−16.44	−0.064	3.70	3.55 (0.54)
7	4POAP_NH@3H_2O	−24.03	−0.095	3.61	3.44 (0.23)
8	4POAP_|@3H_2O	−32.00	−0.008	3.87	3.65 (0.42)
9	4POAP@6H_2O	−59.05	−0.050	3.73	3.58 (0.30)

Finally, both NH and O sites of 4POAP were covered with H_2O, where water vapors accept electronic cloud density from polymer. This intermolecular charge transfer is inbetween those of the individual O and NH interacting systems but is still a very good interaction. The reason behind this is that one group acts as an electron donator while the other accepts as electronic cloud densities which minimize the net charge exchange.

As discussed earlier, H_2O vapor reacts with POAP backbone via either NH or O sites with strong hydrogen bonding. In the case of 4POAP_O@1H_2O, this intermolecular hydrogen bond distance is −8.22 kcal mol^{-1}, which increases upon increasing the number of water vapors, −14.93 kcal mol^{-1} in @2H_2O, and −21.96 kcal mol^{-1} in the case of the 4POAP_O@3H_2O system (Table 2). So, a linear response in interaction energy is observed with number of water vapors. A very similar intermolecular interaction energy is observed in the case of 4POAP_NH@nH_2O systems (Table 2), but here the intermolecular interaction is due to O of H_2O and H of the NH side of the polymer. A −9.03 kcal mol^{-1} interaction energy is simulated for one water vapor, −16.44 kcal mol^{-1}, for two, and −24.03 kcal mol^{-1}, for three, attached to 4POAP. In contrast to the small charge transfer, a good interaction energy of −32 kcal mol^{-1} is simulated between the perpendicularly attached water vapors at a backbone of 4POAP (4POAP_|@3H_2O). On covering all the functional groups (both O and NH) of 4POAP with water vapors, a comparatively higher intermolecular interaction energy of −59.05 kcal mol^{-1} is observed as can be seen from Table 2. But again, the charge transfer is low and the net behavior is an average of O and NH interacting systems. This comparatively higher interaction energy is because of high number of water vapors while the lower charge exchange (−0.05 e^-) is due to the self-interaction and intermolecular hydrogen bonding among H_2O vapors. As explained earlier, the perpendicularly attached H_2O vapors tend to minimize themselves near the O and NH functional groups of 4POAP. So, both the O and NH are responsible for the sensing of H_2O vapors. Furthermore, an electrostatic potential map of these four different interacting systems is given in Figure 3, where the electrophilic and nucleophilic sites can be seen as red and blue region, respectively.

We have also carried out UV−vis absorption spectroscopy for all these four-interacting species, which is given in Figure 4 along with the parent 4POAP as a reference. Three distinct absorption band peaks are simulated in the hydrogen terminated 4POAP; at ca. 427, 361, and 251 nm. The broad absorption band peak at ca. 251 nm has a strong correlation with experimentally reported λ = 258 nm[43,44] which can be assigned to the $\pi \rightarrow \pi^*$ transition of

DOI: 10.1021/acsomega.7b01027
ACS Omega 2017, 2, 6380−6390

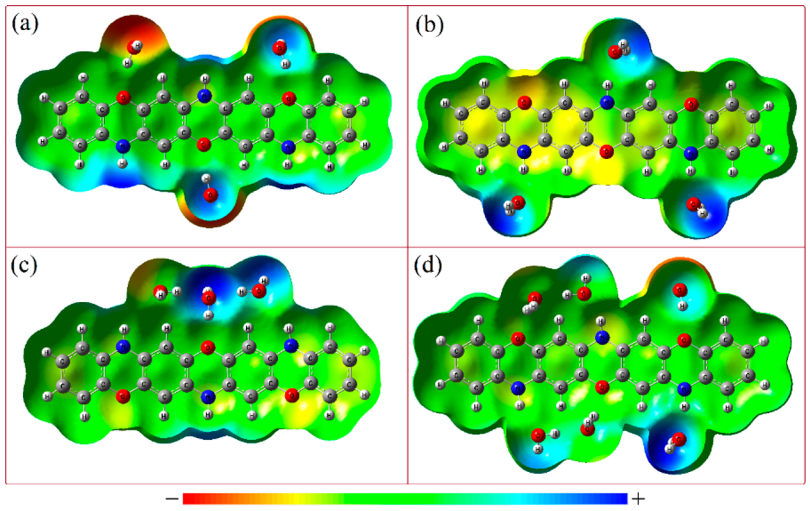

Figure 3. Electrostatic potential map of 4POAP_O@H_2O (a), 4POAP_NH@H_2O (b), 4POAP_|@H_2O (c), and 4POAP@6H_2O (d).

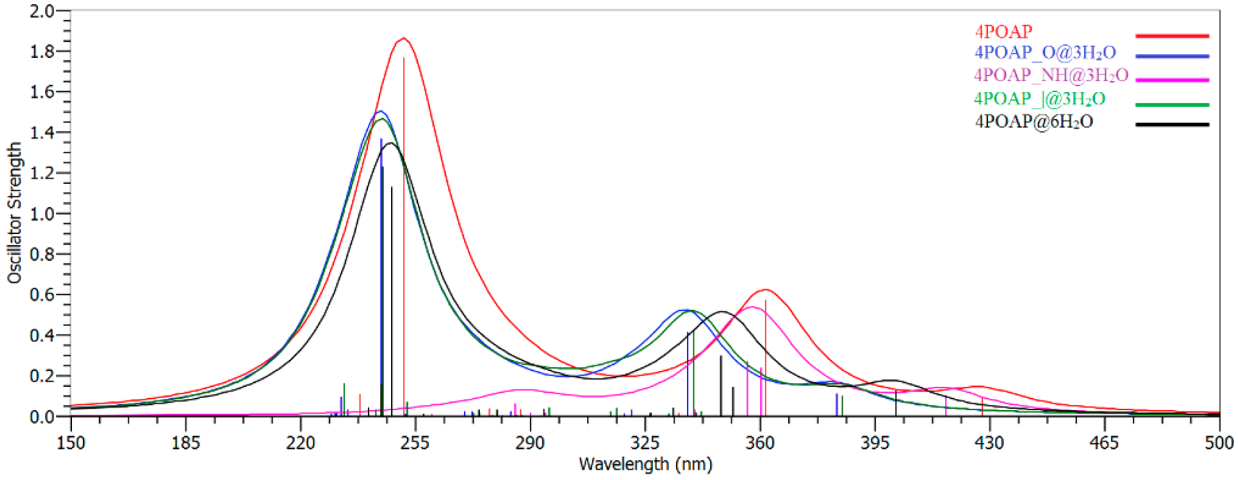

Figure 4. Electronic excitation spectra of 4POAP, where H_2O molecules interact at different sites.

the aromatic benzene unit. On interacting water vapor(s) with 4POAP, all these prominent band peaks are blue-shifted as can be seen from Figure 4 and Table 2. So, water vapor act as a reducing agent which can be seen from the hypsochromic shift in the UV−vis spectra of 4POAP. The HOMO−LUMO band gap of hydrogen terminated 4POAP is 3.54 eV while its first allowed electronic excitation energy is 3.42 eV, as listed in Table 2. The later can be regarded as an optical band gap while the first one is known as electrical band gap. Upon interaction of H_2O vapor at the O side of 4POAP, the band gap elongates and a blue-shifting occurred in the first allowed excitation energy (Table 2). A similar but less pronounced behavior is simulated in case of 4POAP_NH@$n$$H_2O$ systems, where n is the number of H_2O vapors. In these four-interaction systems, the trend of band gap elongation and blue shifting of first allowed electronic excitation energy is because of H_2O vapor(s). So, water vapor(s) cause a hpsochromic shift in POAP; attached either at O, NH, |, or all sides of POAP. So, UV−vis absorption spectroscopy will be the best tool in investigating the humidity sensing behavior of POAP and its oligomers.

As reported by Jeffery et al. 2.2−2.5 Å of hydrogen bonding will be "strong or mostly covalent", 2.5−3.2 Å will be "moderate, mostly electrostatic", while 3.2−4.0 Å is described as "weak, mostly electrostatic". The bonding energy for the strong one should be in the range of −40 to −14 kcal mol^{-1}, for the moderate, −15 to −4 kcal mol^{-1}, and for the weak, <− 4 kcal mol^{-1}.[45]

In summary, POAP senses or reacts to water vapor either at O, NH, or both sites by establishing strong hydrogen (mostly covalent) bonding, although both functional groups have opposite (in term of electron/proton transferring phenomena) but systematic effects. So, the sensing efficiency of the experimentally prepared thin film of POAP and its oligomer will strongly depend on the free availability of O and NH functional groups. Whether the H_2O vapors are in line or perpendicular to its backbone, the reacting sites will be O, NH, or both.

c. Noncovalent Interaction of Water Vapors at the O Site of *n*POAP. After predicting the proper orientation of humidity sensing, different oligomeric chain length of POAP (both reduced and oxidized states) are opted for further simulations. In case of nPOAP_O@H_2O (where n = 2, 4, ..., 10), all available O sites were covered with water vapors. Interaction energy, NBO charge, band gap, and first allowed excitation energy of the respective nPOAP_O@H_2O systems are listed in Table 3. Analysis of the data of Table 3 led us to conclude that water vapor interaction energy with nPOAP is about −7 kcal mol^{-1} per water, where the O of nPOAP donates electronic cloud density toward H_2O. Upon interaction of H_2O vapor with nPOAP, band gap and first allowed excitation energy of the

DOI: 10.1021/acsomega.7b01027
ACS Omega 2017, 2, 6380−6390

Table 3. Interaction Energy (kcal mol^{-1}), NBO Charge (e$^-$), Band Gap (eV), and First Allowed Excitation Energy of *n*POAP_O@H_2O Systems

no.	species	ΔE_{int}	Q_{NBO}	band gap	E_{excit} (eV)
1	**2POAP**			**4.45**	**3.90**
2	2POAP_O@H_2O	−6.96	0.01	4.49	3.93
3	**4POAP**			**3.76**	**3.52**
4	4POAP_O@H_2O	−20.90	0.03	3.83	3.54
5	**6POAP**			**3.29**	**3.21**
6	6POAP_O@H_2O	−35.39	0.05	3.69	3.47
7	**8POAP**			**3.26**	**3.21**
8	8POAP_O@H_2O	−48.65	0.08	3.28	3.28
9	**10POAP**			**3.22**	**3.19**
10	10POAP_O@H_2O	−61.99	0.10	3.23	3.23

resulted complexes increase which is a direct consequence of H_2O adsorption (*vide supra*).

So, along with chain length elongation of POAP, intermolecular interaction energy, NBO charge, band gap, and first allowed electronic excitation energy changes/increases linearly. The HOMO and LUMO energy levels of parent *n*POAP and *n*POAP_O@H_2O are simulated from the density of state (DOS) plots, which are comparatively given in Figure 5. Water vapors change the position of HOMO and LUMO levels of all *n*POAP.

To confirm and elaborate the humidity sensing nature of *n*POAP, UV−vis absorption spectra in the range of 100−600 nm were simulated at the B3LYP/6-31G(d) level of theory. As explained earlier, *n*POAP gives rise to three distinct absorption band peaks. With increasing oligomeric chain length, the third shoulder peak disappears and broadens and shifts the high-energy absorption band peak (~250 nm) toward the visible range (low energy region). UV−vis absorption spectra of the reduced *n*POAP are given in Figure 6 along with *n*POAP_O@H_2O systems.

Analysis of the results of Figure 6 and Table 3 led us to conclude that all the absorption band peaks of parent *n*POAP are sufficiently blue-shifted upon interaction of water vapors which confirm the strong sensing behavior of POAP. This is further supported by the interaction energy, NBO charge, and band gap alteration.

Generally, COPs are positively charged when experimentally synthesized and the cationic form is more reactive than their counterpart neutral state. So, we considered a monocationic *n*POAP without doping agent using UB3LYP/6-31G(d) level of theory. As expected, *n*POAP$^+$ has stronger intermolecular interaction energy with H_2O compared to that of their reduced *n*POAP. The simulated interaction energy is almost double while a similar trend in band gap and first allowed electronic excitation energy is observed. Alteration in band gap and HOMO/LUMO levels of both parent and interacting systems are simulated from DOS, which are given in Figure S4 of the Supporting Information. Interestingly, the charge transferring phenomena is in the opposite direction to that of its reduced form of *n*POAP_O@H_2O systems. All *n*POAP$^+$ has withdrawn electronic cloud density from water molecules as can be seen from Figure 7 and Table 4. In Figure 7, an electrostatic potential map (ESP) of the reduced and cationic form of *n*POAP along with water vapors is given. Different colors are used as a symbol for different values of electrostatic potential; red and blue colors show electron rich and electron deficient (high positivity) regions of the species whereas the green color shows the region of zero potential. A neutral electrostatic potential map for *n*POAP, a nucleophilic one for *n*POAP_O@H_2O, and a slightly electrophilic one for

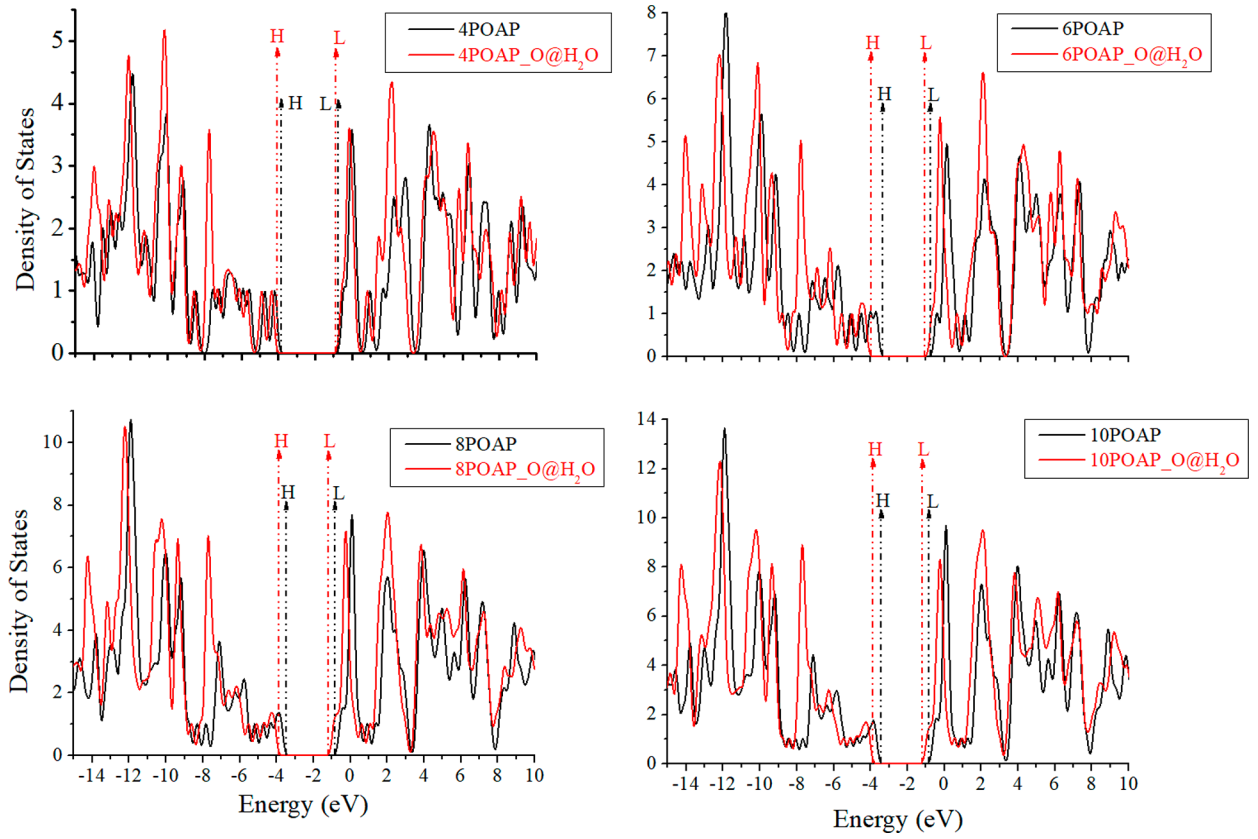

Figure 5. DOS of *n*POAP along with *n*POAP_O@H_2O.

DOI: 10.1021/acsomega.7b01027
ACS Omega 2017, 2, 6380−6390

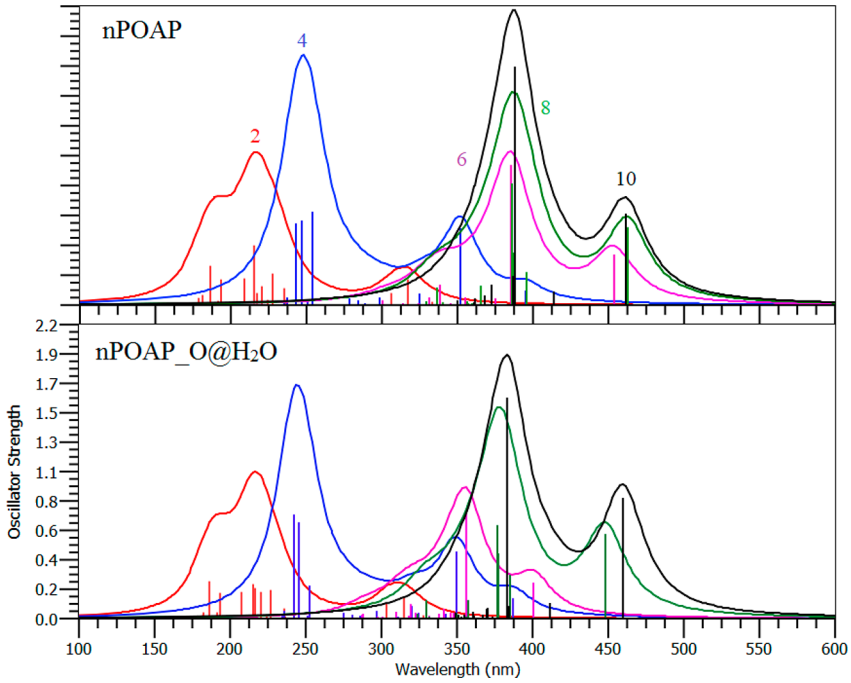

Figure 6. UV−vis absorption spectra of *n*POAP (top) and *n*POAP_O@H_2O (bottom).

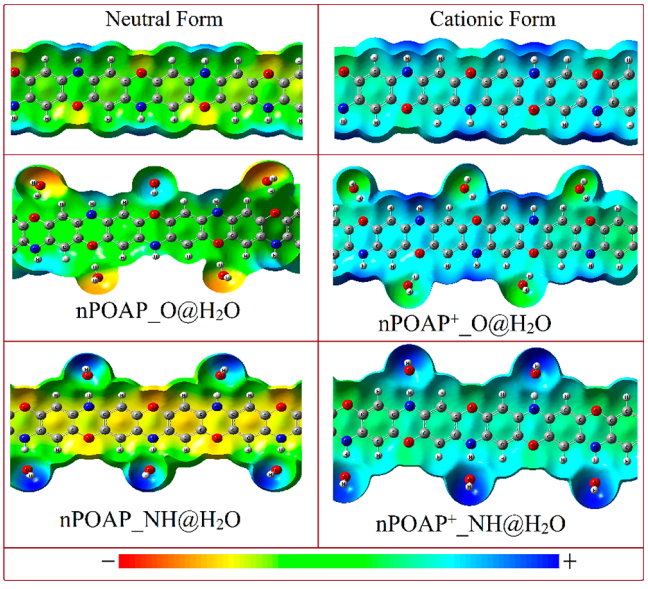

Figure 7. Electrostatic potential map of *n*POAP (both neutral and cationic) along with *n*POAP_NH@H_2O and *n*POAP_O@H_2O systems.

*n*POAP$^+$_O@H_2O can be clearly seen from the electrostatic potential map (Figure 7). On interacting H_2O vapors with *n*POAP, its backbone becomes more electropositive due to the acceptance of proton from H_2O and the corner (especially H_2O attached sides) turned dark yellow (more electronegative).

The proton acceptance/donating ability of water from *n*POAP and *n*POAP$^+$ can also be confirmed from their ESP plots. Both electrostatic potential map and NBO charge analysis strongly corroborate each other (*vide supra*). The UV−vis and UV−vis-near IR spectra of the cationic species along with water vapors are simulated at TD-DFT with UB3LYP/6-31G(d) level of theory. Comparative UV−vis-near IR absorption spectra of *n*POAP$^+$_O@H_2O systems are given in Figure 8, along with that of

Table 4. Interaction Energy (kcal mol^{-1}), NBO Charge (e$^-$), Band Gap (eV), and First Allowed Excitation Energy of *n*POAP$^+$_O@H_2O (at 6-31Gd)

no.	species	ΔE_{int}	Q_{NBO}	band gap	E_{excit} (eV)
1	**2POAP$^+$**			2.56	2.15
2	2POAP$^+$_O@H_2O	−13.99	−0.041	2.54	2.21
3	**4POAP$^+$**			1.03	0.95
4	4POAP$^+$_O@H_2O	−21.35	−0.076	1.07	0.96
5	**6POAP$^+$**			0.47	0.56
6	6POAP$^+$_O@H_2O	−30.12	−0.095	0.51	0.56
7	**8POAP$^+$**			0.32	0.42
8	8POAP$^+$_O@H_2O	−41.98	−0.114	0.38	0.46
9	**10POAP$^+$**			0.21	0.31
10	10POAP$^+$_O@H_2O	−55.41	−0.270	0.23	0.32

parent *n*POAP$^+$. Oxidized *n*POAP has strong UV−vis absorption band peaks in the visible and near IR regions, compared to that of reduced ones. This band shifting to the red or near IR region is because of the formation of a polaronic state, responsible for the high electroactivity. All the absorption band peaks of *n*POAP$^+$ blue shift on interacting with water vapors, which are clearly described in Table 4. As discussed in earlier sections, this blue shifting in the absorption band peaks of *n*POAP$^+$ is due to the interaction of H_2O.

d. Noncovalent Interaction of Water Vapors at the NH Site of *n*POAP. In order to analyze the sensing behavior of the NH site in *n*POAP (both reduced and oxidized), different oligomers are opted for interaction energy, NBO charge, band gap, ESP, and UV−vis spectral characteristics. A comparatively higher intermolecular interaction energy is estimated in case of *n*POAP_NH@H_2O to that of *n*POAP_O@H_2O systems as can be seen from Table 5. The simulated interaction energy for 2POAP_NH@H_2O is −7.65 kcal mol^{-1}, −23.03 kcal mol^{-1} for 4POAP_NH@H_2O, 38.34 kcal mol^{-1} for 6POAP_NH@H_2O, −50.46 kcal mol^{-1} for 8POAP_NH@H_2O, and 68.58 kcal mol^{-1} for 10POAP_NH@H_2O systems. In contrast to the O@H_2O

DOI: 10.1021/acsomega.7b01027
ACS Omega 2017, 2, 6380−6390

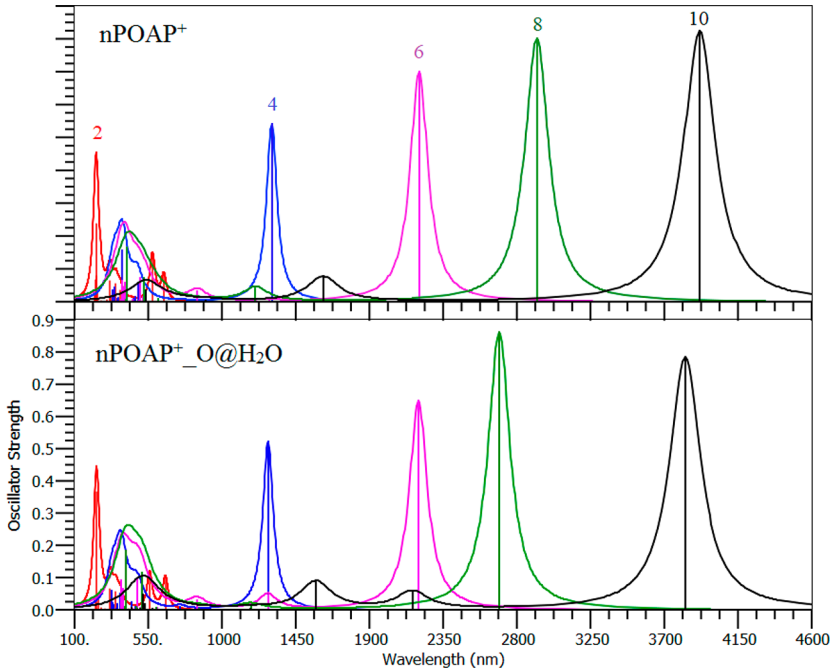

Figure 8. UV−vis-near IR spectra of *n*POAP$^+$ (top) and *n*POAP$^+$_O@H_2O (bottom).

Table 5. Interaction Energy (kcal mol^{-1}), NBO Charge (e$^-$), Band Gap (eV), and First Allowed Excitation Energy of *n*POAP_NH@H_2O

no.	species	ΔE_{int}	Q_{NBO}	band gap	E_{excit} (eV)
1	**2POAP**			**4.45**	**3.90**
2	2POAP_NH@H_2O	−7.65	−0.033	4.34	3.84
3	**4POAP**			**3.76**	**3.52**
4	4POAP_NH@H_2O	−23.03	−0.095	3.63	3.38
5	**6POAP**			**3.29**	**3.21**
6	6POAP_NH@H_2O	−38.34	−0.181	3.21	3.17
7	**8POAP**			**3.26**	**3.21**
8	8POAP_NH@H_2O	−50.46	−0.256	3.14	3.14
9	**10POAP**			**3.22**	**3.19**
10	10POAP_NH@H_2O	−68.58	−0.330	3.10	3.11

interaction, the nature of NH@H_2O is totally different in the case of proton/electron transferring phenomena. Here the NH side of *n*POAP acts as a proton donor, which means the electronic cloud density moves to *n*POAP and results an anionic state. This high interaction energy and charge transferring are responsible for strong hydrogen bonding (H−O) between H of NH and O of H_2O in all *n*POAP_NH@H_2O systems. Compared to *n*POAP_O@H_2O systems, here the amount of charge transfer is 3-fold which make the *n*POAP backbone more nucleophilic and H_2O vapor more electrophilic. This phenomenon can be clearly seen from the ESP plots (Figure 7) where the yellowish region depicts the electronegative nature and the bluish is that of electropositive character (H_2O sides). This time, the band gap and first allowed electronic excitation energy decrease upon interaction with H_2O vapors as can be seen from Table 5. So, here water act as an oxidizing agent which finally validate the acid/base chemistry of water in different reagents (*vide supra*).

The band gap of 2POAP decreases from 4.45 to 4.34 eV, a decrease of 0.13 eV in 4POAP, 0.08 eV in 6POAP, 0.12 eV in 8POAP, and again a decrease of 0.12 eV in 10POAP is observed upon sensing H_2O vapors. The shifting of HOMO and LUMO energy levels in *n*POAP after interacting with H_2O are also very prominent as can be seen from the DOS plot, given in Figure 9. These band shiftings are clear evidence toward the high sensitivity of *n*POAP for H_2O vapors. Moreover, UV−vis absorption spectra of all these interacting species are simulated which are comparatively given in Figure 10 along with isolated *n*POAP. Absorption band peaks of all *n*POAP are red-shifted upon interaction with H_2O, as can be seen from Table 5 and Figure 10. Water vapor has increased the visible light absorption capability of all POAP oligomers (shift the λ_{max} to lower energy region) which further supports and confirms POAP as the best sensor for humidity.

Again, comparatively higher intermolecular interaction energies are observed in all *n*POAP$^+$_NH@H_2O systems, which are listed in Table 6. In contrast to the reduced state, here water vapors have caused a blue-shifting in all the oxidized oligomers of POAP. This behavior in all POAP$^+$ oligomers can be analyzed from the blue shifting of UV−vis and UV−vis-near IR absorption band peaks (Figure 11). Being a universal species, water interacts with POAP either in reduced or oxidized state. For clarity reasons, the first allowed electronic excitation band peaks of all these isolated and H_2O interacting *n*POAP$^+$ systems are listed in Table 6. However, the charge transferring phenomena is in the same direction as that of *n*POAP_NH@H_2O systems but more prominent. In the case of a reduced state (*n*POAP), the electronic cloud density was moved to *n*POAP due to NH functional groups (electrophilic nature). Here the proton donating nature of *n*POAP$^+$ toward H_2O vapors is because of the oxidized state (cationic form). So, upon interaction with H_2O vapors, the oxidized states are reduced as can be visualized from the ESP plot (Figure 7), band gap enlargement, and shifting of HOMO/LUMO levels (Figure S5).

The opposite interacting nature of O and NH functional groups with H_2O vapors can be precisely seen from Figure 12, where the red and blue-shifting of λ_{max} is shown. So, water vapor can be detected at either site (O, NH, or both) of POAP. The strong humidity sensing ability of POAP is stem to the free availability of these two functional groups which simultaneously

DOI: 10.1021/acsomega.7b01027
ACS Omega 2017, 2, 6380−6390

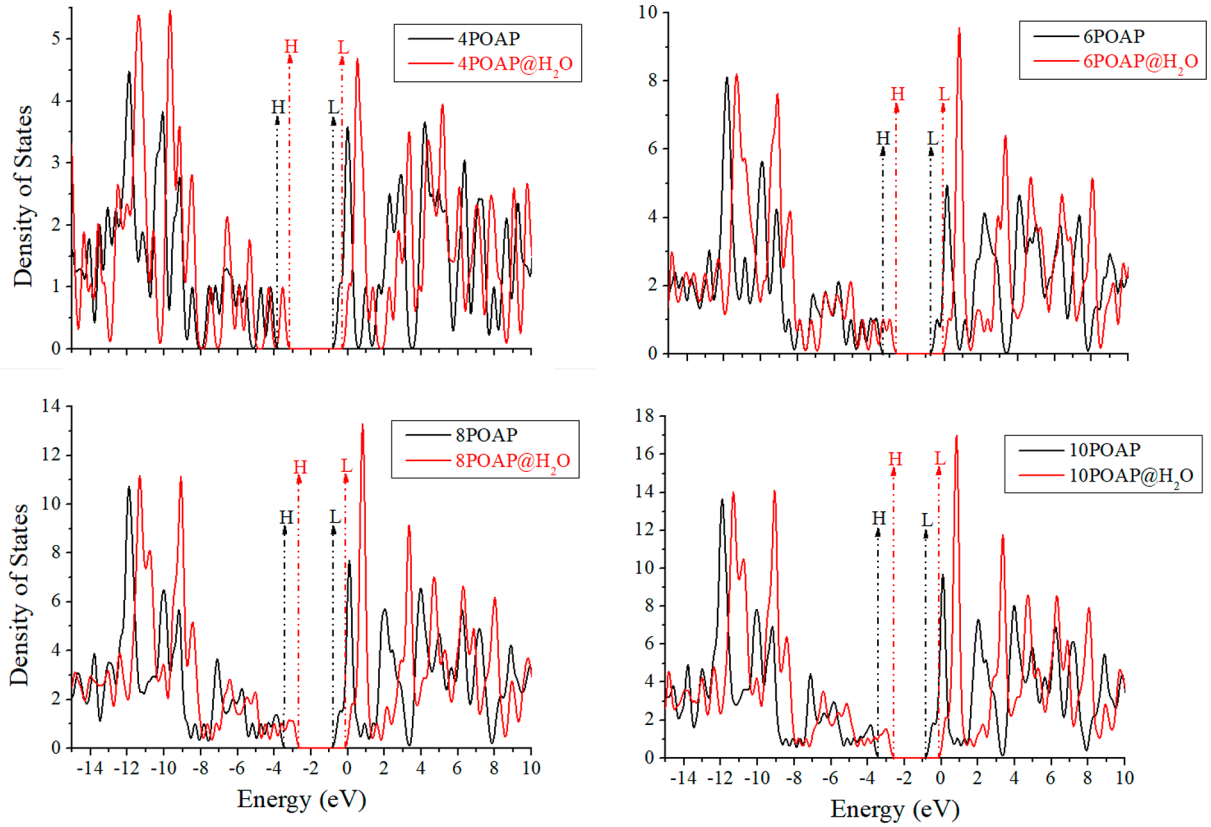

Figure 9. DOS of *n*POAP along with *n*POAP_NH@H_2O.

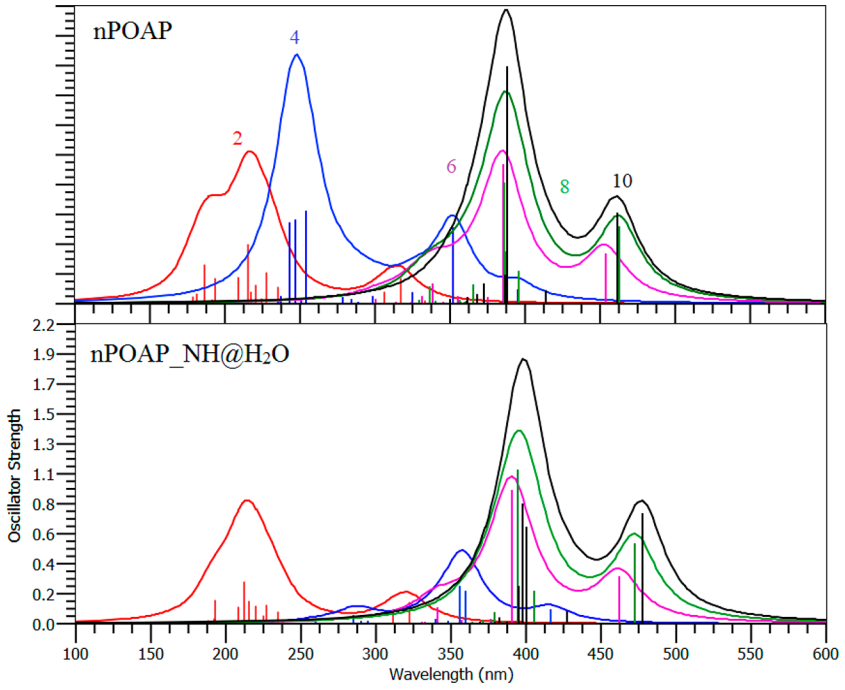

Figure 10. UV−vis absorption spectra of *n*POAP (top) and *n*POAP_NH@H_2O (bottom).

act as a proton donor/acceptor agents, followed by redox chemistry of H_2O.

3. CONCLUSION

The prominent nature of poly(*o*-aminophenol) (PAOP) among all CPs is because of its redox conducting nature, ladderlike molecular structure, and availability of more reactive sites such as O and NH functional groups on its polymeric backbone. Due to the free availability of these functional groups, POAP can be used as a best candidate for gas sensing. We have carried out a systematic theoretical study for a POAP gas sensor; considering its O and NH functional groups as attacking sites for H_2O vapors.

DOI: 10.1021/acsomega.7b01027
ACS Omega 2017, 2, 6380−6390

Table 6. Interaction Energy (kcal mol^{-1}), NBO Charge (e^{-}), Band Gap (eV), and First Allowed Excitation Energy of *n*POAP^{+}_NH@H_2O (6-31/G)

no.	species	ΔE_{int}	Q_{NBO}	band gap	E_{excit} (eV)
1	2POAP^{+}			2.56	2.15
2	2POAP^{+}_NH@H_2O	−20.52	−0.049	2.66	2.18
3	4POAP^{+}			1.03	0.95
4	4POAP^{+}_NH@H_2O	−48.56	−0.117	1.16	1.02
5	6POAP^{+}			0.47	0.56
6	6POAP^{+}_NH@H_2O	−71.60	−0.221	0.60	0.64
7	8POAP^{+}			0.32	0.42
8	8POAP^{+}_NH@H_2O	−94.87	−0.309	0.42	0.49
9	10POAP^{+}			0.21	0.31
10	10POAP^{+}_NH@H_2O	−115.46	−0.380	0.25	0.37

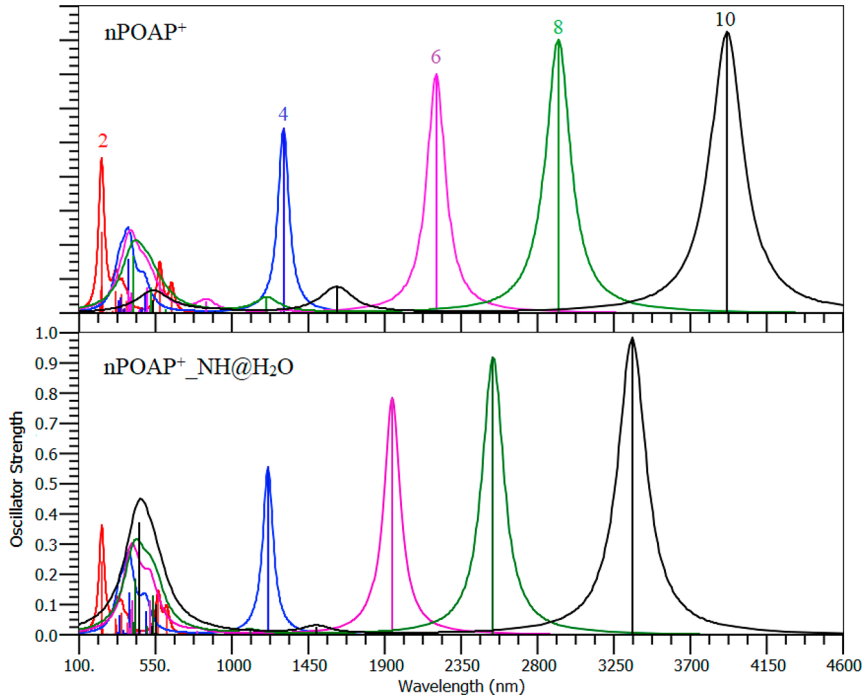

Figure 11. UV−vis-near IR spectra of *n*POAP^{+} (top) and *n*POAP^{+}_NH@H_2O (bottom).

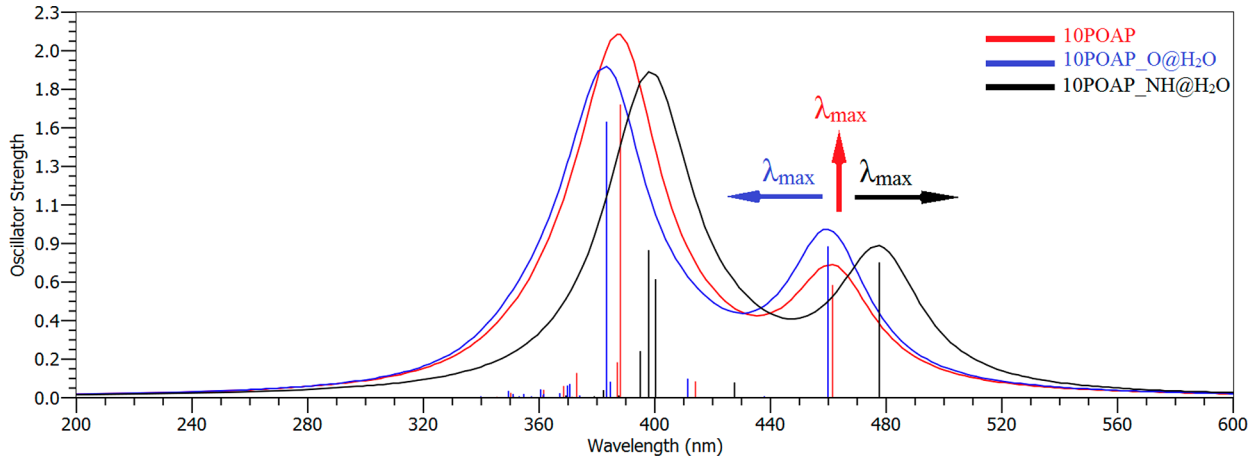

Figure 12. UV−vis spectra of 10POAP@H_2O at O and NH sites.

For theoretical simulations, DFT and time-dependent DFT simulations are performed at the various level of theories. DFT at the B3LYP/6-31G(d) level of theory is found to be the best method for theoretical study of PAOP and its interacting systems with different analytes. In summary, POAP both in reduced and oxidized states has strong sensing ability toward H_2O vapors which is estimated from good interaction energy, as a consequence the strong hydrogen bonding is more likely covalent.

DOI: 10.1021/acsomega.7b01027
ACS Omega 2017, 2, 6380−6390

Furthermore, structural distortion (change in geometric parameters), charge exchange, shifting of HOMO and LUMO levels, band gap alteration, and perturbation in UV−vis spectra absorption band peaks of POAP upon interacting with H_2O validate its sensing ability. Finally, if one side of POAP acts as a proton donor then the other will act as a proton acceptor, which further strengthens its intermolecular interaction; however, the NH position of the polymer is energetically favorable compared to the O site toward H_2O_{vap}. It is concluded that H_2O is responsible for blue-shifting in λ_{max} of POAP UV−vis spectra, so color change in the thin film of POAP may be a direct method for detection.

4. COMPUTATIONAL METHODS

The ground-state geometries of *n*POAP oligomers (where $n = 2, 4, ..., 10$) were simulated using hybrid DFT at the B3LYP functional (Becke three parameter, Lee, Yang, and Parr)[46] with the 6-31G(d) basis set. B3LYP and its unrestricted formulism, such as UB3LYP, are used for the reduced (POAP) and oxidized ($POAP^+$) form of POAP, respectively.[47] From the last two decades, this level of theory has been proven to accurately describe π-conjugated systems such as CPs and other conjugated materials.[48−50] All calculations were performed using Gaussian 09,[51] while the results are analyzed through Gabedit[52] and Gauss view.[53] Prior to sensor study of *n*POAP, its symmetrical trimer (hydrogen terminated) is employed for the testing of an appropriate level of theory. Molecular gas phase H_2O is considered as water vapors. Water vapors are interacted at the NH and O sites and perpendicular to the polymeric backbone of 4POAP, considering both reduced and oxidized states. After the systematic study, *n*POAP (*n*POAP and $nPOAP^+$) is interacted with water vapors. $POAP^+$ oligomers either isolated or in complex state ($nPOAP^+@H_2O$) are positively charged with doublet spin, and the simulations were performed at the UB3LYP/6-31G(d) level of theory. No symmetry constraint was applied during geometry optimization.[54] Harmonic frequency calculations were performed to confirm the optimized structures with no negative frequencies. Intermolecular interaction energies were also simulated to study the interaction behavior of polymer with H_2O. This was further confirmed by natural bond orbital (NBO) analysis. Frontier molecular orbitals such as highest occupied molecular orbital (HOMO), lowest unoccupied molecular orbital (LUMO), and their respective band gap calculations were also carried out at the mentioned level of theory. UV−vis absorption spectra are also simulated to understand the sensing behavior of polymers. Both the gas phase and solvent media of acetonitrile using polarized continuum model (PCM) are employed. In case of POAP oligomers, both solvent and gas phase UV−vis spectra were almost similar (see Figure S6), so, in order to reduce the computational cost, the gas phase simulations are considered. Finally, the oligomeric properties were extrapolated to obtain polymeric properties through a second-order polynomial fit equation.[55]

■ ASSOCIATED CONTENT

Supporting Information

The Supporting Information is available free of charge on the ACS Publications website at DOI: 10.1021/acsomega.7b01027.

Optimized geometric structures, DOS, and UV−vis spectra of *n*POAP and $nPOAP@H_2O$ systems (PDF)

■ AUTHOR INFORMATION

Corresponding Authors

*E-mail: anwarulhaqalishah@uop.edu.pk (A.A.S.).
*E-mail: salmabilal@uop.edu.pk. Tel.: +92(091) 9216652, 9216701-20. Fax: +92(091) 9216652 (S.B.).

ORCID

Anwar-ul-Haq Ali Shah: 0000-0002-4991-5194
Habib Ullah: 0000-0001-9290-0265

Notes

The authors declare no competing financial interest.

■ ACKNOWLEDGMENTS

We acknowledge the Higher Education Commission (HEC) Islamabad, Pakistan, for financial support under research grant nos. 20-1647 and 20-3111/NRPU/R&D/HEC.

■ REFERENCES

(1) Janata, J.; Josowicz, M. Conducting Polymers in Electronic Chemical Sensors. *Nat. Mater.* **2003**, *2*, 19−24.
(2) Liu, G.; Xun, S.; Vukmirovic, N.; Song, X.; Olalde-Velasco, P.; Zheng, H.; Battaglia, V. S.; Wang, L.; Yang, W. Polymers with Tailored Electronic Structure for High Capacity Lithium Battery Electrodes. *Adv. Mater.* **2011**, *23*, 4679−4683.
(3) Alberti, G.; Casciola, M.; Massinelli, L.; Bauer, B. Polymeric Proton Conducting Membranes for Medium Temperature Fuel Cells (110−160 °C). *J. Membr. Sci.* **2001**, *185*, 73−81.
(4) Bae, B.; Yoda, T.; Miyatake, K.; Uchida, H.; Watanabe, M. Proton-Conductive Aromatic Ionomers Containing Highly Sulfonated Blocks for High-Temperature-Operable Fuel Cells. *Angew. Chem., Int. Ed.* **2010**, *49*, 317−320.
(5) Kim, Y. H.; Sachse, C.; Machala, M. L.; May, C.; Müller-Meskamp, L.; Leo, K. Highly Conductive PEDOT:PSS Electrode with Optimized Solvent and Thermal Post-Treatment for Ito-Free Organic Solar Cells. *Adv. Funct. Mater.* **2011**, *21*, 1076−1081.
(6) Yu, Z.; Zhang, Q.; Li, L.; Chen, Q.; Niu, X.; Liu, J.; Pei, Q. Highly Flexible Silver Nanowire Electrodes for Shape-Memory Polymer Light-Emitting Diodes. *Adv. Mater.* **2011**, *23*, 664−668.
(7) Jiang, W.; Yu, D.; Zhang, Q.; Goh, K.; Wei, L.; Yong, Y.; Jiang, R.; Wei, J.; Chen, Y. Ternary Hybrids of Amorphous Nickel Hydroxide−Carbon Nanotube-Conducting Polymer for Supercapacitors with High Energy Density, Excellent Rate Capability, and Long Cycle Life. *Adv. Funct. Mater.* **2015**, *25*, 1063−1073.
(8) Zeng, X. Y.; Zhang, Q. K.; Yu, R. M.; Lu, C. Z. A New Transparent Conductor: Silver Nanowire Film Buried at the Surface of a Transparent Polymer. *Adv. Mater.* **2010**, *22*, 4484−4488.
(9) Huang, J.; Virji, S.; Weiller, B. H.; Kaner, R. B. Nanostructured Polyaniline Sensors. *Chem. - Eur. J.* **2004**, *10*, 1314−1319.
(10) Wang, L. R.; Ran, F.; Tan, Y. T.; Zhao, L.; Kong, L. B.; Kang, L. Coral Reef-Like Polyanaline Nanotubes Prepared by a Reactive Template of Manganese Oxide for Supercapacitor Electrode. *Chin. Chem. Lett.* **2011**, *22*, 964−968.
(11) Yang, K.; Xu, H.; Cheng, L.; Sun, C.; Wang, J.; Liu, Z. In Vitro and in Vivo Near-Infrared Photothermal Therapy of Cancer Using Polypyrrole Organic Nanoparticles. *Adv. Mater.* **2012**, *24*, 5586−5592.
(12) Kim, Y.; Cook, S.; Tuladhar, S. M.; Choulis, S. A.; Nelson, J.; Durrant, J. R.; Bradley, D. D.; Giles, M.; McCulloch, I.; Ha, C.-S.; Ree, M. A Strong Regioregularity Effect in Self-Organizing Conjugated Polymer Films and High-Efficiency Polythiophene: Fullerene Solar Cells. *Nat. Mater.* **2006**, *5*, 197−203.
(13) Behzadi, M.; Noroozian, E.; Mirzaei, M. A Novel Coating Based on Carbon Nanotubes/Poly-Ortho-Phenylenediamine Composite for Headspace Solid-Phase Microextraction of Polycyclic Aromatic Hydrocarbons. *Talanta* **2013**, *108*, 66−73.
(14) Ehsani, A.; Mahjani, M. G.; Jafarian, M.; Naeemy, A. Influence of Ionic Surfactant on Physio-Electrochemical Properties and Fractal

DOI: 10.1021/acsomega.7b01027
ACS Omega 2017, 2, 6380−6390

Dimension of Poly Ortho Aminophenol Film. *Prog. Org. Coat.* **2010**, *69*, 510−516.
(15) Sakai, Y.; Sadaoka, Y.; Matsuguchi, M. Humidity Sensors Based on Polymer Thin Films. *Sens. Actuators, B* **1996**, *35*, 85−90.
(16) Zhu, Z.-T.; Mason, J. T.; Dieckmann, R.; Malliaras, G. G. Humidity Sensors Based on Pentacene Thin-Film Transistors. *Appl. Phys. Lett.* **2002**, *81*, 4643−4645.
(17) Chen, Z.; Lu, C. Humidity Sensors: A Review of Materials and Mechanisms. *Sens. Lett.* **2005**, *3*, 274−295.
(18) Lawrence, M. G. The Relationship between Relative Humidity and the Dewpoint Temperature in Moist Air: A Simple Conversion and Applications. *Bull. Am. Meteorol. Soc.* **2005**, *86*, 225−233.
(19) Kuang, Q.; Lao, C.; Wang, Z. L.; Xie, Z.; Zheng, L. High-Sensitivity Humidity Sensor Based on a Single SnO_2 Nanowire. *J. Am. Chem. Soc.* **2007**, *129*, 6070−6071.
(20) Zhang, Y.; Yu, K.; Jiang, D.; Zhu, Z.; Geng, H.; Luo, L. Zinc Oxide Nanorod and Nanowire for Humidity Sensor. *Appl. Surf. Sci.* **2005**, *242*, 212−217.
(21) Gradon, L.; Clark, A. B.; Seakins, P. J. Infrared gas analyser and humidity sensor. US Patent US 5468961 A, 1995.
(22) Romain, A.-C.; Nicolas, J.; Andre, P. In *Seminars in Food Analysis* **1997**; Vol. 2, p 283−296.
(23) Bai, H.; Shi, G. Gas Sensors Based on Conducting Polymers. *Sensors* **2007**, *7*, 267−307.
(24) Hwang, L.; Ko, J.; Rhee, H.; Kim, C. A Polymer Humidity Sensor. *Synth. Met.* **1993**, *57*, 3671−3676.
(25) Ullah, H.; Shah, A. A.; Bilal, S.; Ayub, K. DFT Study of Polyaniline NH_3, CO_2, and CO Gas Sensors: Comparison with Recent Experimental Data. *J. Phys. Chem. C* **2013**, *117*, 23701−23711.
(26) Bibi, S.; Ullah, H.; Ahmad, S. M.; Ali Shah, A. A.; Bilal, S.; Tahir, A. A.; Ayub, K. Molecular and Electronic Structure Elucidation of Polypyrrole Gas Sensors. *J. Phys. Chem. C* **2015**, *119*, 15994−16003.
(27) Ullah, H.; Ayub, K.; Ullah, Z.; Hanif, M.; Nawaz, R.; Bilal, S.; Shah, A. H. A. Theoretical Insight of Polypyrrole Ammonia Gas Sensor. *Synth. Met.* **2013**, *172*, 14−20.
(28) Nohria, R.; Khillan, R. K.; Su, Y.; Dikshit, R.; Lvov, Y.; Varahramyan, K. Humidity Sensor Based on Ultrathin Polyaniline Film Deposited Using Layer-by-Layer Nano-Assembly. *Sens. Actuators, B* **2006**, *114*, 218−222.
(29) Lin, Q.; Li, Y.; Yang, M. Polyaniline Nanofiber Humidity Sensor Prepared by Electrospinning. *Sens. Actuators, B* **2012**, *161*, 967−972.
(30) Jain, S.; Chakane, S.; Samui, A.; Krishnamurthy, V.; Bhoraskar, S. Humidity Sensing with Weak Acid-Doped Polyaniline and Its Composites. *Sens. Actuators, B* **2003**, *96*, 124−129.
(31) Tonosaki, T.; Oho, T.; Isomura, K.; Ogura, K. Effect of the Protonation Level of Poly (*O*-Phenylenediamine) (POPD) on the Ac Impedance of Humidity-Sensitive POPD/Poly (Vinyl Alcohol) Composite Film. *J. Electroanal. Chem.* **2002**, *520*, 89−93.
(32) Ogura, K.; Tonosaki, T.; Shiigi, H. Ac Impedance Spectroscopy of Humidity Sensor Using Poly (*O*-Phenylenediamine)/Poly (Vinyl Alcohol) Composite Film. *J. Electrochem. Soc.* **2001**, *148*, H21−H27.
(33) Suri, K.; Annapoorni, S.; Sarkar, A.; Tandon, R. Gas and Humidity Sensors Based on Iron Oxide−Polypyrrole Nanocomposites. *Sens. Actuators, B* **2002**, *81*, 277−282.
(34) Zhang, T.; He, Y.; Wang, R.; Geng, W.; Wang, L.; Niu, L.; Li, X. Analysis of DC and AC Properties of Humidity Sensor Based on Polypyrrole Materials. *Sens. Actuators, B* **2008**, *131*, 687−691.
(35) Geng, W.; Li, N.; Li, X.; Wang, R.; Tu, J.; Zhang, T. Effect of Polymerization Time on the Humidity Sensing Properties of Polypyrrole. *Sens. Actuators, B* **2007**, *125*, 114−119.
(36) Parvatikar, N.; Jain, S.; Khasim, S.; Revansiddappa, M.; Bhoraskar, S.; Prasad, M. A. Electrical and Humidity Sensing Properties of Polyaniline/WO_3 Composites. *Sens. Actuators, B* **2006**, *114*, 599−603.
(37) Salavagione, H. J.; Arias-Pardilla, J.; Pérez, J.; Vázquez, J.; Morallón, E.; Miras, M. C.; Barbero, C. Study of Redox Mechanism of Poly (*O*-Aminophenol) Using in Situ Techniques: Evidence of Two Redox Processes. *J. Electroanal. Chem.* **2005**, *576*, 139−145.
(38) Bilal, S.; Bibi, S.; Ahmad, S. M.; Shah, A. H. A. Counterpoise-Corrected Energies, NBO, HOMO−LUMO and Interaction Energies of Poly (*O*-Aminophenol) for Ammonia Sensing by DFT Methods. *Synth. Met.* **2015**, *209*, 143−149.
(39) Valdes García, M. a. A. V.; Tunon Blanco, P. T.; Ivaska, A. A Poly (O-Aminophenol) Modified Electrode as an Amperometric Hydrogen Peroxide Biosensor. *Electrochim. Acta* **1998**, *43*, 3533−3539.
(40) Li, J.; Zhao, J.; Wei, X. A Sensitive and Selective Sensor for Dopamine Determination Based on a Molecularly Imprinted Electropolymer of *O*-Aminophenol. *Sens. Actuators, B* **2009**, *140*, 663−669.
(41) Tucceri, R.; Arnal, P. M.; Scian, A. N. Spectroscopic Characterization of Poly (Ortho-Aminophenol) Film Electrodes: A Review Article. *ISRN Polym. Sci.* **2012**, *2012*, 1−26.
(42) Shah, A. H. A.; Holze, R. Poly (*O*-Aminophenol) with Two Redox Processes: A Spectroelectrochemical Study. *J. Electroanal. Chem.* **2006**, *597*, 95−102.
(43) Zhang, A.; Cui, C.; Chen, Y.; Lee, J. Synthesis and Electrochromic Properties of Poly-*O*-Aminophenol. *J. Electroanal. Chem.* **1994**, *373*, 115−121.
(44) Tucceri, R.; Barbero, C.; Silber, J.; Sereno, L.; Posadas, D. Spectroelectrochemical Study of Poly-*O*-Aminophenol. *Electrochim. Acta* **1997**, *42*, 919−927.
(45) Jeffrey, G. A. *An Introduction to Hydrogen Bonding*; Oxford University Press: New York, 1997; pp 1−303.
(46) Becke, A. D. Density-Functional Exchange-Energy Approximation with Correct Asymptotic Behavior. *Phys. Rev. A: At., Mol., Opt. Phys.* **1988**, *38*, 3098.
(47) Alemán, C.; Ferreira, C. A.; Torras, J.; Meneguzzi, A.; Canales, M.; Rodrigues, M. A.; Casanovas, J. On the Molecular Properties of Polyaniline: A Comprehensive Theoretical Study. *Polymer* **2008**, *49*, 5169−5176.
(48) Ullah, H.; Shah, A.-u.-H. A.; Bilal, S.; Ayub, K. Doping and Dedoping Processes of Polypyrrole: DFT Study with Hybrid Functionals. *J. Phys. Chem. C* **2014**, *118*, 17819−17830.
(49) Ullah, H.; Shah, A. A.; Ayub, K.; Bilal, S. Density Functional Theory Study of Poly (*O*-Phenylenediamine) Oligomers. *J. Phys. Chem. C* **2013**, *117*, 4069−4078.
(50) Zade, S. S.; Bendikov, M. From Oligomers to Polymer: Convergence in the Homo− Lumo Gaps of Conjugated Oligomers. *Org. Lett.* **2006**, *8*, 5243−5246.
(51) (a) Frisch, M. J.; Trucks, G. W.; Schlegel, H. B.; Scuseria, G. E.; Robb, M. A.; Cheeseman, J. R.; Scalmani, G.; Barone, V.; Mennucci, B.; Petersson, G. A.; et al. *Gaussian 09*, Rev. D. 0.1; Gaussian, Inc.: Wallingford, CT, 2013. (b) *Gaussian 09*, Rev. A. 02, Gaussian, Inc.: Wallingford, CT, 2013; *200*.
(52) Allouche, A. R. Gabedit—A Graphical User Interface for Computational Chemistry Softwares. *J. Comput. Chem.* **2011**, *32*, 174−182.
(53) Dennington, R. D.; Keith, T. A.; Millam, J. M. *Gaussview 5.0.8*; Gaussian Inc, 2008.
(54) Yanai, T.; Tew, D. P.; Handy, N. C. A New Hybrid Exchange−Correlation Functional Using the Coulomb-Attenuating Method (CAM-B3LYP). *Chem. Phys. Lett.* **2004**, *393*, 51−57.
(55) Zade, S. S.; Bendikov, M. From Oligomers to Polymer: Convergence in the HOMO-LUMO Gaps of Conjugated Oligomers. *Org. Lett.* **2006**, *8*, 5243−5246.

DOI: 10.1021/acsomega.7b01027
ACS Omega 2017, 2, 6380−6390